Supplementary Information

One-Step Method to Fabricate Novel Three-Dimensional GaP Nanopore Arrays for Enhanced Photoelectrochemical Hydrogen Production

Pengjie Liu,[a] Maojun Zheng,[*ab] Qiang Li,[a] Liguo Ma,[a] Faze Wang,[a] Dongkai Jiang,[a] Jingnan Song,[a] Yuxiu You,[a] Li Ma,[c] and Wenzhong Shen[a]

a. Key Laboratory of Artificial Structure and Quantum Control, Ministry of Education, School of Physics and Astronomy, Shanghai Jiao Tong University, Shanghai, 200240, People's Republic of China.

b. Collaborative Innovation Center of Advanced Microstructures, Nanjing, 210093, People's Republic of China.

c. School of Chemistry and Chemical Technology, Shanghai Jiao Tong University, Shanghai 200240, People's Republic of China

** Author to whom correspondence should be addressed. Electronic mail: mjzheng@sjtu.edu.cn*

Experimental section

Materials

All chemicals used in this study wereanalytical grade and were used as received without further purification. Deionized water was used in all cases for making solutions. Single crystal n-GaP (111) wafers (300 μm thick) doped with sulfur at concentration of $(3\sim6)\times10^{17}$ cm^{-3} were obtained from GRINM. The wafer was diced into 8 mm × 8mm squares and degreased by sonicating in acetone and ethanol, followed by rinsing in deionized water. Indium film was deposited on the sample back surface by direct current magnetron sputtering for Ohmic contacts. Then high purity silver paint was smeared on the In film in order to establish an electrical contact with a copper plate. The copper plate was painted with epoxy to ensure that only the GaP sample was in contact with the electrolyte. Then the copper plate with the sample was pressed in an O-ring of an electrochemical cell leaving 0.48 cm^2 sample exposed to the electrolyte.

Preparation of 3D GaP NPs

Well-ordered 3D GaP NPs were fabricated on the GaP wafer substrate via one-step electrochemical etching. A two-electrode set-up was used for electrochemical etching. The GaP sample and graphite electrode were used as the anodic and cathodic electrode, respectively. Electrochemical etching was carried out in 1M NaBr aqueous solution in darkness at 4 ℃ under a polarization voltage. The etching voltage was increased with a scan rate of 20 mV/s from 0 to 25 V, then was held for different time (t_c) to obtain nanopores with different length. The GaP sample turned from orange to yellow after etching. For comparison, we also prepared GaP NPs by anodic etching GaP in 1M HBr electrolyte.

Materials Characterization

The morphologies of the as-grown 3D GaP NPs were observed by a field emission scanning electron microscope (FESEM; Zeiss Ultra Plus). The XRD patterns of the samples were obtained by an X-ray diffractometer (XRD; D8 ADVANCE X-ray diffractometer, Bruker, Karlsruhe, Germany) with Cu K_α radiation (λ = 0.154 nm). The reflectance spectrum was measured by using a Lambda 750S spectrometer (Perkin-Elmer) consisting of a deuterium and tungsten-halogen lamp, photomultiplier, and integrating sphere with 60 mm. The room-temperature photoluminescence (PL) spectra of the samples were recorded using the Jobin Yvoon LabRam HR 800 UV system with an excitation wavelength of 325 nm.

Photoelectrochemical Measurements

The PEC performances were evaluated in a typical three-electrode electrochemical cell configuration (a Ag/AgCl reference electrode, 3D GaP NPs working electrode and a Pt mesh counter electrode) using an electrochemical workstation (PARSTAT 4000) in 0.35 M Na_2S and 0.25 M Na_2SO_3 (pH=13.35) solution. All three electrodes were immersed in a glass cell with a quartz window, through which the working electrode was illuminated under simulated solar light (AM 1.5G, 100 mW/cm^2) by a solar simulator (SOLARDGE 700). For a typical J-V measurement, the potential was swept linearly from -1.5 to -1 V vs Ag/AgCl at scan rate of 20 mV/s. The chronoamperometry measurement was evaluated under the same illumination at a fixed potential of -1 V vs Ag/AgCl with 60s light on/off switch. Potentials were reported as measured versus Ag/AgCl and as calculated versus RHE using the Nernstian relation $E_{RHE} = E_{Ag/AgCl} + 0.059 \times pH + E°_{Ag/AgCl}$, where E_{RHE} is the convert potential versus RHE, $E_{Ag/AgCl}$ is the experimental potential measured against the Ag/AgCl reference electrode, and $E°_{Ag/AgCl}$ is the standard potential of Ag/AgCl at 25 ℃ (0.1976 V). The EIS data were collected under 1 sun illumination at OCP (open circuit potential) with AC perturbation amplitude of 10 mV in the frequency range from 10^5 to 10^{-1} Hz. The flat potential were determined using Mott-Schottky analyses at fixed frequency of 1 kHz in darkness.

Mechanism of Hydrogen Generation

Because the Na_2S and Na_2SO_3 were used as the sacrificial reagent, the total reaction in the PEC system is different the reaction of water splitting consisting of HER and OER. The mechanism of hydrogen production can be explained through the following equations.[1]

In the anodic compartment:

$$2S^{2-} + 2h^+ \rightarrow S_2^2 \quad (1)$$

$$S_2^{2-} + SO_3^2 \rightarrow S_2O_3^{2-} + S^{2-} \quad (2)$$

$$S^{2-} + SO_3^{2-} + 2h^+ \rightarrow S_2O_3^{2-} \quad (3)$$

$$SO_3^{2-} + 2OH^- + 2h^+ \rightarrow SO_4^{2-} + H_2O \quad (4)$$

$$2SO_3^{2-} + 2h^+ \rightarrow S_2O_6^{2-} \quad (5)$$

In the cathodic compartment:

$$2H^+ + 2e^- \rightarrow H_2 \quad (6)$$

As illustrated in Fig. 1e, the photogenerated holes (h^+) and electron (e^-) originate from the electron transition as the n-GaP is illuminated. The holes move to the surface of GaP to participate in the reactions (1)-(5), and electron move to the counter electrode-Pt through the external circuit to participate in the reaction (6). So as the cathodic compartment of the total reaction, hydrogen evolution could be promoted simultaneously with the anodic reactions.

Reason for Disappearance of Irregular Nucleation Layer

The disappearance of the irregular nucleation layer could be attributed to the polarization etching voltage, which increased with a scan rate of 20 mV/s from 0 V to 25 V during the etching process. Fig. S6a is the SEM images of GaP sample etched under constant voltage. It is clear that the irregular nucleation layer is on the top, so a few of nanopore could be observed. We stopped the etching when the voltage was increasing and the morphologies of the sample were shown in the Fig. S6. We can see that part of the irregular nucleation was lifted off and the triangular nanopore arrays were exposed. That is to say, the polarization etching voltage could lift off the irregular nucleation layer during the etching process.

Reason for the phenomenon that the onset potential and the flat band of the GaP NPs shifted oppositely

Firstly, the onset potential does not only depend on the flat band, but also the overpotential. As discussed in the Ref. 2, in the case of hematite, the onset potential of +0.9 V is substantially anodic of the flat-band potential (+0.4 V). This large overpotential is thought to be caused mainly from the slow kinetics for water oxidation that results in hole accumulation at the surface, and then subsequent surface recombination occurs until sufficiently positive potentials are achieved for appreciable charge transfer across the interface.[2,3]

In the Ref. 4 (RSC Adv., 2015, 5, 61021-61030), the hematite/electrolyte charge transfer resistance of different samples were similar (Fig. 2c in Ref. 4). That is to say, the transfer of holes from the semiconductor to the electrolyte in different samples was similar.[4] So the onset potentials had the same trend with flat band potential because the the samples had similar kinetics and overpotentials.

In our case, the nanostructures did not only change the flat band, but also the overpotential. On the one hand, consistent with Ref. 5, the GaP nanostructures caused the flat band to shift positively. On the other hand, the nanostructures could decrease the overpotential.[6,7] The electrochemical impedance spectroscopy (EIS) of 3D GaP NPs and planar GaP (Fig. 4c) showed that nanostructures can significantly facilitate the faster interfacial charge transfer and more efficient charge separation, resulting in lower overpotential. So even the flat band of the 3D GaP NPs were more positive than that of planar samples, the onset potential is more negative than that of planar samples.

Table S1 Comparison table on PEC performance of the 3D GaP NPs and classic photoanodes

Ref No.	Materials	Onset Potential (V vs RHE)	ABPE (%)
This work	3D GaP NPs	-0.58	2.95
8	CdS	-0.31	No data
9	TiO2/CdS/Co–Pi	0.14	0.47
10	CdSe/CdS@ZnO	No data	0.98
11	BiVO4	0.69	No data
12	InP	-0.22	0.95

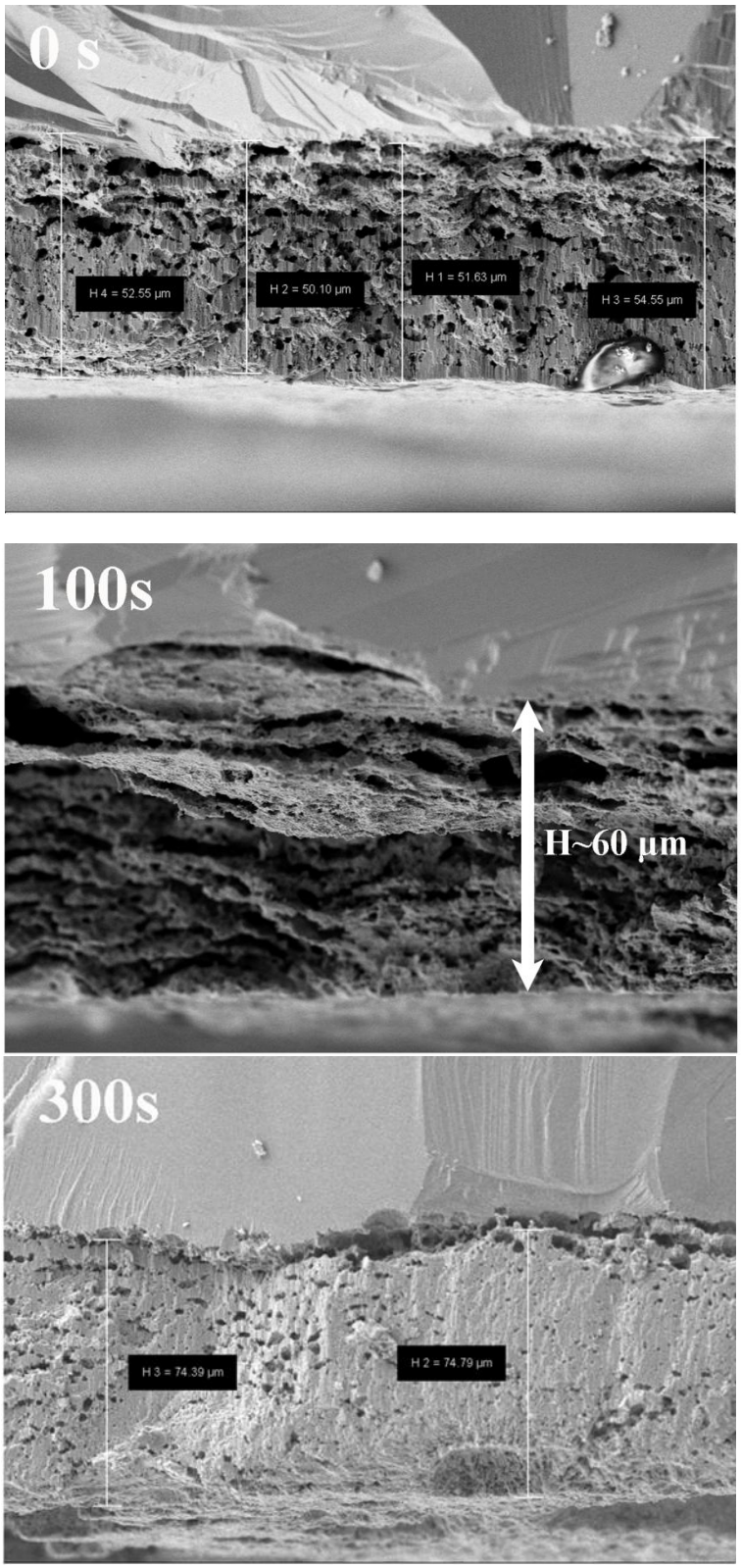

Fig.S1 Global cross-sectional SEM images of samples showing the nanopore lengths.

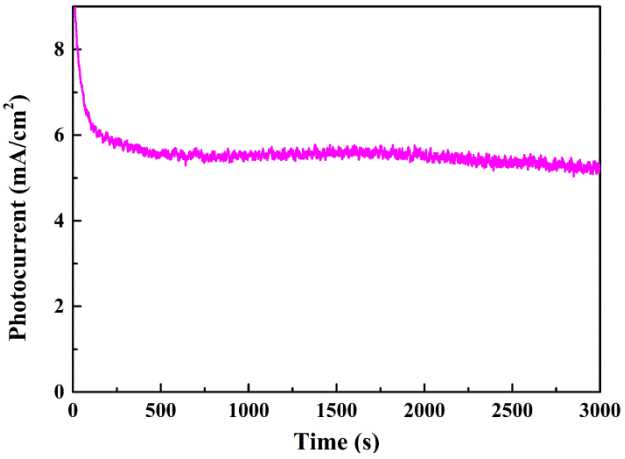

Fig. S2 Current density under constant light illumination (100 mW/cm^2) versus time (stability performance) of 3D GaP NPs (100s) measured at 0 V vs RHE.

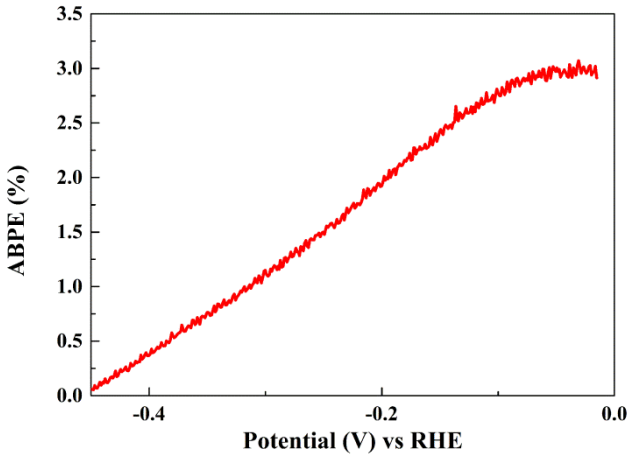

Fig. S3 Calculated photoconversion efficiencies. (ABPE, Applied Bias Photon-to-current Efficiency)

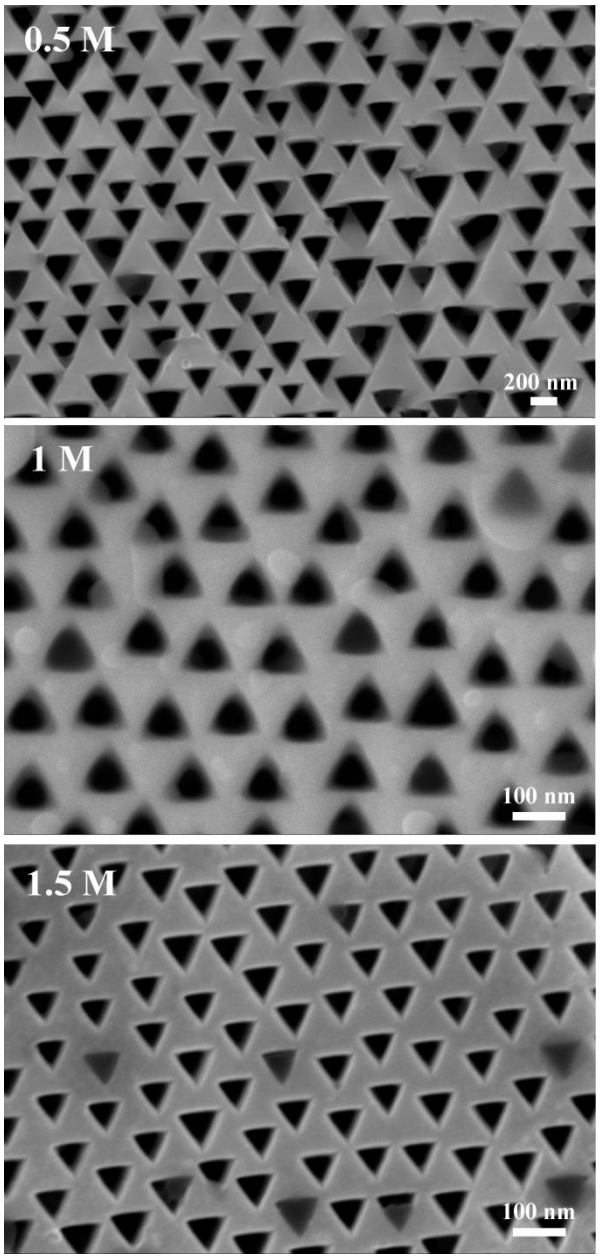

Fig. S4 SEM images of nanopores etched in solution with different concentration.

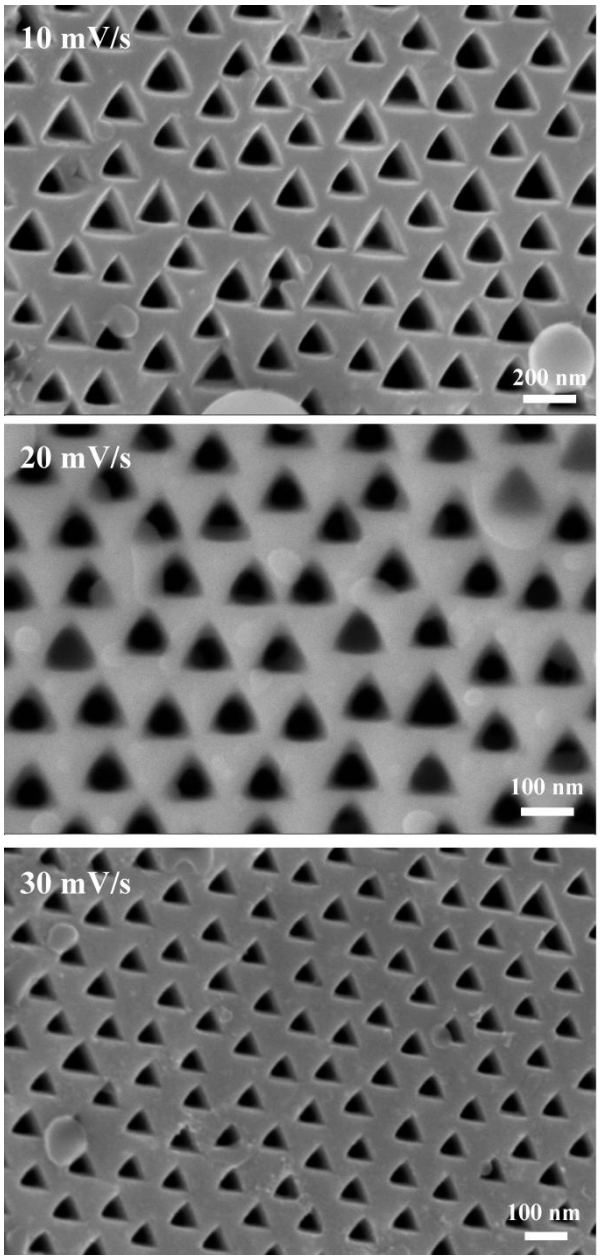

Fig. S5 SEM images of nanopores etched with different scan rate.

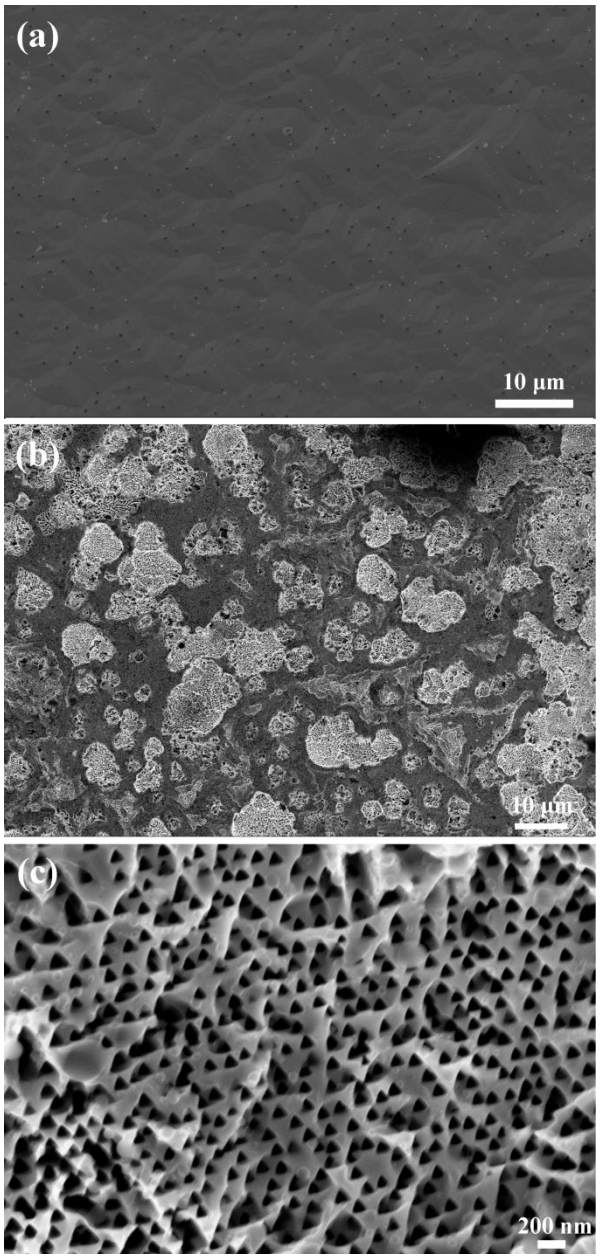

Fig. S6 Evolution of the surface morphology during the etching process.

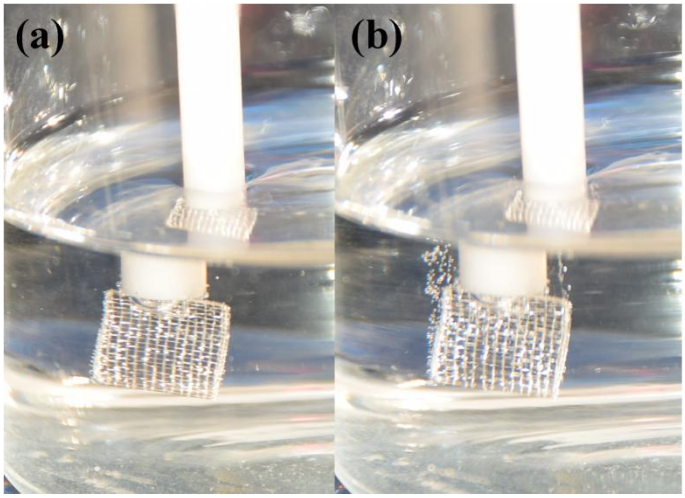

Fig. S7 Bubbles on the Pt electrode in the three-electrode system as the work electrode (0 V vs RHE) was (a) planar wafer or (b) 3D GaP NPs (100s).

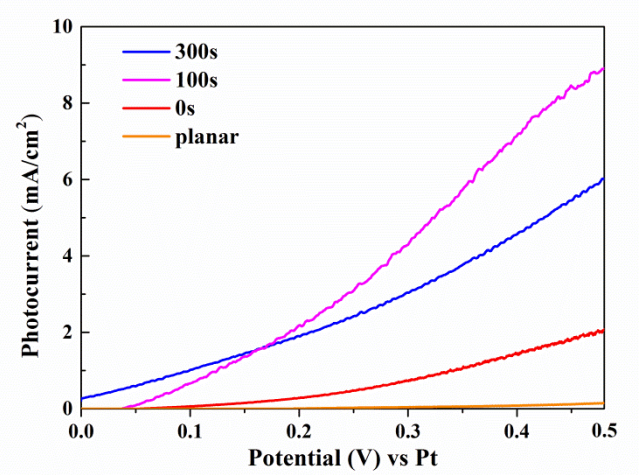

Fig. S8 Photocurrent density vs bias voltage curves of the 3D GaP NPs with different etching time and planar wafer under illumination of 100 mW/cm^2 in the two-electrode system.

References

1 S. Banerjee, S. K. Mohapatra, P. P. Das and M. Misra, *Chem. Mater.,* 2008, 20, 6784-6791.

2 S. D. Tilley, M. Cornuz, K. Sivula, and M. Grätzel, *Angew. Chem. Int. Ed.*, 2010, **49**, 6405-6408.

3 D. Cao, W. Luo, J. Feng, X. Zhao, Z. Li, and Z. Zou, *Energy Environ. Sci.*, 2014, **7**, 752-759.

4 B. Iandolo, H. Zhang, B. Wickman, I. Zoric, G. Conibeer, and A. Hellman, *RSC Adv.*, 2015, **5**, 61021-61030.

5 L. Santinacci, A-M. Gonçalves, N. Simon, and A. Etcheberry, *Electrochim. Acta*, 2010, **56**, 878-888.

6 M. S. Faber, R. Dziedzic, M. A. Lukowski, N. S. Kaiser, Q. Ding, and S. Jin, *J. Am. Chem. Soc.*, 2014, **136**, 10053-10061.

7 J. Oh, T. G. Deutsch, H. C. Yuan, and H. M. Branz, *Energy Environ. Sci.*, 2011, **4**, 1690-1694.

8 W. Kim, M. Seol, H. Kim, J. B. Miller, A. J. Gellman, and K. Yong, *J. Mater. Chem. A*, 2013, **1**, 9587-9589.

9 G. Ai, H. Li, S. Liu, R. Mo, and J. Zhong, *Adv. Funct. Mater.*, 2015, **25**, 5706–5713.

10 H. Kim and K. Yong, *Appl. Phys. Lett.*, 2013, **103**, 223903.

11 E. Alarcón-Lladó, L. Chen, M. Hettick, N. Mashouf, Y. Lin, A. Javey, and J. W. Ager, *Phys. Chem. Chem. Phys.*, 2014, **16**, 1651-1657.

12 Q. Li, M. Zheng, L. Ma, M. Zhong, C. Zhu, B. Zhang, F. Wang, J. Song, L. Ma and W. Shen, *ACS Appl. Mater. Inter.*, 2016, **8**, 22493- 22500.